Available online at www.sciencedirect.com
ScienceDirect
Tetrahedron
Tetrahedron 63 (2007) 11399–11409

Enantiomeric products formed via different mechanisms: asymmetric hydrogenation of an α,β-unsaturated carboxylic acid involving a $Ru(CH_3COO)_2$[(*R*)-binap] catalyst

Masahiro Yoshimura, Yoshitaka Ishibashi, Kengo Miyata, Yuhki Bessho, Masaki Tsukamoto and Masato Kitamura*

Research Center for Materials Science and the Department of Chemistry, Nagoya University, Chikusa, Nagoya 464-8602, Japan

Received 8 August 2007; revised 22 August 2007; accepted 22 August 2007
Available online 26 August 2007

Abstract—Hydrogenation of (*Z*)-3-phenyl-2-butenoic acid with a $Ru(CH_3COO)_2$[(*R*)-binap] (BINAP=2,2′-bis(diphenylphosphino)-1,1′-binaphthyl) catalyst in methanol gives (*S*)-3-phenyl-2-butanoic acid and its *R* enantiomer in a 97:3 (4 atm) to 94:6 (100 atm) ratio in quantitative yield. Both hydrogen gas and protic methanol participate in the saturation of the olefinic bond. Analysis of the products obtained using (*Z*)-3-phenyl-2-butenoic acid-3-^{13}C and either H_2, a 1:1 H_2–D_2 mixture, or D_2 in CH_3OD indicates that several catalytic cycles are operative, showing different reactivity and stereoselectivity. The major *S* enantiomer was formed primarily by the standard Ru monohydride mechanism, whereas the minor *R* isomer is produced via more complicated routes.

1. Introduction

Asymmetric catalysis involves the multistep conversion of a prochiral substrate into an enantiomerically-enriched chiral product. The enantioselectivity has generally been analyzed as being due to competing diastereomorphic catalytic cycles utilizing a chiral catalyst, in which the ratio of the enantiomeric products is determined by the relative stabilities of the diastereomeric transition states of the first irreversible step, according to the Arrhenius equation.[1] In most cases, however, the primary presupposition, namely the operation of a single mechanism, has not been confirmed.[2] We have long suspected that in some cases, two enantiomers may be produced via entirely different pathways, instead of the diastereomorphically identical mechanism. A notable example is the BINAP–Ru-catalyzed hydrogenation of geraniol to citronellol.[3,4] The minor enantiomer is derived via initial isomerization of the allylic alcohol to a homoallylic alcohol, γ-geraniol, wherein the two olefinic isomers exhibit opposite enantioselection.[5] Certain (*E*)-α-(acylamino)acrylic esters undergo *E*/*Z* isomerization in the presence of chiral phosphine catalysts in alcohols.[6] Hydrogenation of imines catalyzed by a chiral titanocene[7] also involves prior *syn*/*anti* isomerization of the substrates. Thus, in these cases, the minor enantiomers are derived more or less from isomeric substrates formed during the reaction.[8] More generally, however, it is not unreasonable to assume that a reaction system contains several potentially active species that can catalyze reaction of the same substrate but with different reactivity and stereoselectivity, in either sense or extent. In a given catalytic system, these cycles are linked by various reaction parameters and, therefore, the observed enantioselectivity is the average of the contribution of these different mechanistic cycles. The following fully details a clear example of asymmetric catalysis giving enantiomers from the same substrate by different mechanisms.[9,10]

2. Results and discussion

2.1. Asymmetric hydrogenation of (*Z*)-3-phenyl-2-butenoic acid catalyzed by (*R*)-BINAP–Ru diacetate

(*Z*)-3-Phenyl-2-butenoic acid [(*Z*)-**2**] was selected as substrate and $Ru(CH_3COO)_2$[(*R*)-binap] [(*R*)-**1**] as catalyst. The standard hydrogenation conditions were [(*R*)-**1**]=0.5 mM, [(*Z*)-**2**]=100 mM (substrate/catalyst ratio (S/C)=200), solvent=methanol, and temperature=30 °C. Reaction at 4 atm H_2 quantitatively gave (*S*)-3-phenylbutanoic acid [(*S*)-**4**] in 94% enantiomeric excess (ee). The enantioselectivity was sensitive to the H_2 pressure. The ee of 94%, obtained for the 1–4 atm range decreased to 92% ee at 50 atm, and to 88% ee at 100 atm. As might be expected,

Keywords: Asymmetric hydrogenation; BINAP–Ru; α,β-Unsaturated carboxylic acid; Minor enantiomeric product; Mechanism.
* Corresponding author. Tel.: +81 52 789 2957; fax: +81 52 789 2261; e-mail: kitamura@os.rcms.nagoya-u.ac.jp

0040–4020/$ - see front matter © 2007 Elsevier Ltd. All rights reserved.
doi:10.1016/j.tet.2007.08.071

however, the reaction *rate* was enhanced with an increase in hydrogen pressure.[2,11–13]

The substrate (*Z*)-**2** is stable and does not undergo geometrical or positional isomerization during the course of the hydrogenation.[14] For comparison, hydrogenation of (*E*)-**2** in methanol at 4 atm and 10–25 °C for 25 h gave (*R*)-**4** in 5% ee and 97% yield.[15] Notably, the *E* isomer readily isomerizes to **3**.[16] This β,γ-unsaturated carboxylic acid was hydrogenated with (*R*)-**1** in methanol under similar conditions (S/C=200, 1.5 atm, 10–25 °C, 2 h) to afford (*S*)-**4** in 74% ee.[15]

When (*R*)-**1** was reacted with an excess of (*Z*)-**2**, ligand exchange occurred smoothly to afford crystalline Ru[(*Z*)-$CH_3(C_6H_5)C{=}CHCOO]_2$[(*R*)-binap] [(*R*)-**5**].[17–19] The molecular structure is described in Section 4. Over the course of the hydrogenation of (*Z*)-**2**, no substantial change was seen in the ^1H and ^{31}P NMR spectra of the reaction mixture. Ru hydrides were undetectable when reacting (*R*)-**1** and (*Z*)-**2** under an H_2 atmosphere.

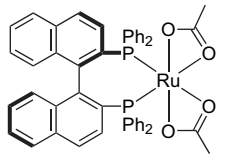

(*R*)-**1**

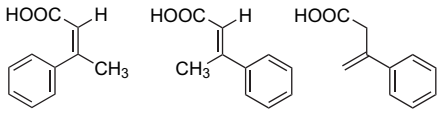

(*Z*)-**2** (*E*)-**2** **3**

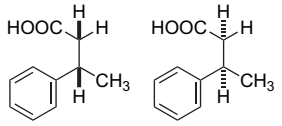

(*S*)-**4** (*R*)-**4**

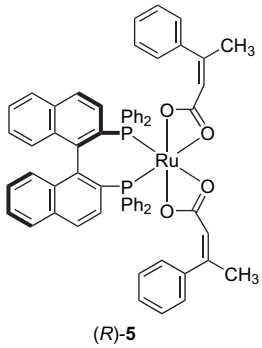

(*R*)-**5**

2.2. Isotopic labeling experiments

Comparison of the enantiomeric products obtained via reaction using H_2, D_2, and a 1:1 mixture of H_2 and D_2 provides useful information regarding the mechanism. To further insure the accuracy of the measurement of the isotopomer ratios, the ^{13}C-labeled substrate, (*Z*)-3-phenyl-2-butenoic acid-3-^{13}C [(*Z*)-**2**-3-^{13}C], was used for the hydrogenation. The experiments were carried out in CH_3OD using (*R*)-**1** as the catalyst, and varying the hydrogen pressure from 4 to 100 atm. The reactions using H_2 and the H_2–D_2 mixture were stopped upon 6–22% conversion to minimize complications caused by gas/solvent and gas/gas isotope exchange.[2,20] Fortunately, isotope exchange is significantly retarded by the presence of the substrate, and the extent of the observed scrambling does not affect the mechanistic argument. The hydrogenation product was a mixture of eight isotopomers, (*S*)-**4**-*h*,*h*-3-^{13}C, (*S*)-**4**-*h*,*d*-3-^{13}C, (2*R*,3*S*)-**4**-*d*,*h*-3-^{13}C, (2*R*,3*S*)-**4**-*d*,*d*-3-^{13}C, (*R*)-**4**-*h*,*h*-3-^{13}C, (*R*)-**4**-*h*,*d*-3-^{13}C, (2*S*,3*R*)-**4**-*d*,*h*-3-^{13}C, and (2*S*,3*R*)-**4**-*d*,*d*-3-^{13}C.[21] Deuterium was not doubly incorporated at C(2). The *S* and *R* enantiomers of **4** were separated by preparative HPLC on a chiral stationary phase and subjected to $^{13}C\{^1H,^2H\}$–^1H correlation NMR and $^{13}C\{^1H,^2H\}$ NMR analyses to determine the structure and the ratio of the four isotopomers, respectively. The relative stereochemistry of **4**-*d*,*h*-3-^{13}C was determined by ^1H NMR analysis. Reference (2*R**,3*S**)-**4**-*d*,*h* and (2*S**,3*S**)-**4**-*d*,*h*[21] samples were prepared by diimide reduction of (*Z*)-**2**-2-*d* and (*E*)-**2**-2-*d*, respectively, and occurred with complete cis stereochemistry.[22] Both the product and substrate were isotopically stable under the reaction conditions. Table 1 summarizes the product analysis.

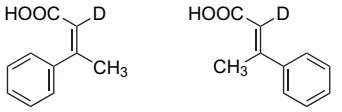

(*Z*)-**2**-2-*d* (*E*)-**2**-2-*d*

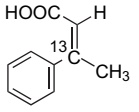

(*Z*)-**2**-3-^{13}C

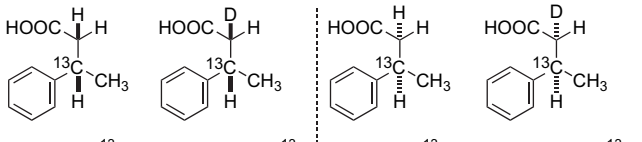

(*S*)-**4**-*h*,*h*-3-^{13}C (2*R*,3*S*)-**4**-*d*,*h*-3-^{13}C (*R*)-**4**-*h*,*h*-3-^{13}C (2*S*,3*R*)-**4**-*d*,*h*-3-^{13}C

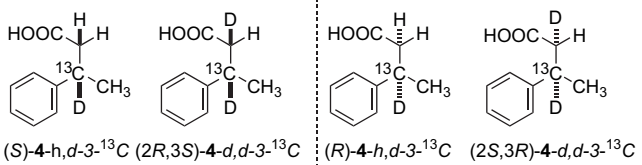

(*S*)-**4**-h,*d*-3-^{13}C (2*R*,3*S*)-**4**-*d*,*d*-3-^{13}C (*R*)-**4**-*h*,*d*-3-^{13}C (2*S*,3*R*)-**4**-*d*,*d*-3-^{13}C

Of note, the saturation of the olefinic bond of (*Z*)-**2**-3-^{13}C utilizes both hydrogen gas and protic methanol. Thus, the reaction using H_2 in CH_3OD at 4–100 atm gave **4** containing 98.5–95% protium at C(2), while the protium content at C(3) ranges from 12% (4 atm) to 25% (10 atm) to 47% (50 atm) and 60.5% (100 atm). This trend was also the case when using an H_2–D_2 mixture, giving a 49–43% protium content at C(2) and 7% (4 atm), 23% (50 atm), and 26% (100 atm) protium content at C(3). An increase in hydrogen pressure enhanced the degree of contribution of gaseous hydrogen. The extent of methanol participation was

Table 1. Analysis of **4**-3-^{13}C obtained by isotopic labeling experiments using (*Z*)-**2**-3-^{13}C and $Ru(CH_3COO)_2$[(*R*)-binap] [(*R*)-**1**][a] in CH_3OD[b]

Conditions	H_2, atm				H_2–D_2, atm			D_2, atm
	4	10	50	100	4	50	100	4
Time	9 h	10 h	10 min	7 min	9 h	12 min	7 min	35.2 h
Gas analysis, %								
H_2	98.0	98.7	99.7	99.8	49.0	44.0	48.6	0
HD	2.0	1.3	0.3	0.2	2.3	0.3	2.0	2.0
D_2	0	0	0	0	48.7	55.7	49.4	98.0
Solvent analysis, %								
CH_3OH	<1	<1	<1	<1	<1	<1	<1	1
CH_3OD	>99	>99	>99	>99	>99	>99	>99	99
Conversion, %	10	10	16	22	17	10	6	99.9
(*S*)-**4**/(*R*)-**4**[c]	97:3	97:3	95.5:4.5	94:6	97:3	96:4	94:6	97:3
Protium incorporation, %								
H in C(2)	98.5	98.1	96.5	95	49	43	48	0
H in C(3)	12	24.7	47	60.5	7	23	26	1
Product distribution, %								
Major enantiomer								
(*S*)-**4**-*h*,*h*-3-^{13}C	10.3	22.7	44.5	57.4	3.1	9.3	12.8	0
(*S*)-**4**-*h*,*d*-3-^{13}C	88.7	75.8	52.4	37.8	45.9	32.1	35.1	0
(2*R*,3*S*)-**4**-*d*,*h*-3-^{13}C	0.0	0.5	1.0	1.1	3.1	11.9	11.7	1.1
(2*R*,3*S*)-**4**-*d*,*d*-3-^{13}C	1.0	1.0	2.1	3.7	47.9	46.7	40.4	98.9
Minor enantiomer								
(*R*)-**4**-*h*,*h*-3-^{13}C	53.3	56.7	72.9	82.2	23.3	24.4	30.0	0
(*R*)-**4**-*h*,*d*-3-^{13}C	30.0	26.7	15.5	9.3	20.1	15.6	16.7	0
(2*S*,3*R*)-**4**-*d*,*h*-3-^{13}C	16.7	16.6	11.1	7.8	13.3	17.8	18.3	0
(2*S*,3*R*)-**4**-*d*,*d*-3-^{13}C	0.0	0.0	0.5	0.7	43.3	42.2	35.0	>99.9

[a] The detailed procedures for the reaction and analysis are described in Section 4.
[b] CH_3OD contained 0.5% of CH_3OH. D_2 gas contained 0.4% of HD.
[c] The ratio was determined by HPLC analysis.

greater than for the hydrogenation of enamides reported previously.[2,13]

Reaction at 4 atm of H_2 in CH_3OD afforded (*S*)-**4** in 94% ee, consisting of (*S*)-**4**-*h*,*h*-3-^{13}C, (*S*)-**4**-*h*,*d*-3-^{13}C, (2*R*,3*S*)-**4**-*d*,*h*-3-^{13}C, and (2*R*,3*S*)-**4**-*d*,*d*-3-^{13}C in a 10.3:88.7:0:1.0 ratio. With 1:1 H_2–D_2 in CH_3OD, the distribution was changed to 3.1:45.9:3.1:47.9.

At 50 atm, the major *S* product decreased to 95.5%. Increase in hydrogen pressure enhanced the degree of contribution of gaseous hydrogen. This trend is more significant at 100 atm. In addition, the isotope incorporation pattern varied significantly. The isotopomer ratio of (*S*)-**4**-*h*,*h*-3-^{13}C, (*S*)-**4**-*h*,*d*-3-^{13}C, (2*R*,3*S*)-**4**-*d*,*h*-3-^{13}C, and (2*R*,3*S*)-**4**-*d*,*d*-3-^{13}C becomes 44.5:52.4:1.0:2.1 (50 atm) and 57.4:37.8:1.1:3.7 (100 atm) using H_2 in CH_3OD, and further changes to 9.3:32.1:11.9:46.7 (50 atm) and 12.8:35.1:11.7:40.4 (100 atm) for H_2–D_2 in CH_3OD. The reaction using D_2 and CH_3OD gave mostly **4**-*d*,*d*-3-^{13}C as expected.

Hydrogenation in CH_3OH at 4–100 atm gave (*S*)-**4** in 94–88% ee. Neither the reaction with D_2 nor CH_3OD demonstrated any isotope effects on enantioselectivity. Most notably, the major *S* enantiomer and the minor *R* enantiomer displayed different isotopic labeling patterns. The hydrogen pressure also affected the product distribution. Of note are the distribution patterns in going from H_2 to H_2–D_2 as shown in Table 1—the major *S* enantiomer obtained with H_2 at 4 atm in CH_3OD was **4**-*h*,*d*-3-^{13}C (88.7%), which is followed by **4**-*h*,*h*-3-^{13}C (10.3%) and **4**-*d*,*d*-3-^{13}C (1.0%). In contrast, the *R* enantiomer consisted of **4**-*h*,*h*-3-^{13}C (53.3%), **4**-*h*,*d*-3-^{13}C (30.0%), and **4**-*d*,*h*-2-^{13}C (16.7%). Hydrogenation at 100 atm resulted in the *S* product containing **4**-*h*,*d*-3-^{13}C and **4**-*h*,*h*-3-^{13}C in comparable amounts, 37.8% and 57.4%, respectively, while the *R* enantiomer contains largely **4**-*h*,*h*-3-^{13}C (82.2%) together with other isotopomers. The minor *R* enantiomer appears to utilize more gaseous hydrogen than the major *S* isomer. Use of a 1:1 mixture of H_2 and D_2 led to different distributions of the isotopomers, as discussed below in terms of mechanistic models.

2.3. Possible catalytic cycles

Reaction of phosphine–Ru(II) complexes and hydrogen generates a variety of Ru hydrides depending on the reaction conditions (solvent, acidity/basicity, H_2 pressure, etc.), which catalyze homogeneous hydrogenation of olefinic substrates.[23,24] Heterolytic cleavage of molecular hydrogen results in Ru monohydrides but, upon reaction with additional hydrogen molecules, Ru polyhydrides are also produced. The reactivity and enantioselectivity in asymmetric hydrogenation are highly influenced by hydrogen pressure, among other parameters.[2,11,13,23] This is due to either a change of the major catalytic species, or alternation of the mechanistic pathway, or both. The pressure effect is particularly significant in BINAP–Ru-catalyzed hydrogenation of unsaturated carboxylic acids.[23] This and earlier studies on the BINAP–Ru-catalyzed hydrogenation suggest the operation of at least the three sets of cycles, as shown in Figure 1. The carboxylates attached to Ru act as either monodentate or bidentate ligands, while methanol may coordinate to the metallic center to stabilize the complexes.[25]

The cycles designated $\boldsymbol{S_1}$ and $\boldsymbol{R_1}$ are the standard mechanism for BINAP–Ru-catalyzed hydrogenation of α,β-unsaturated carboxylic acids, as elucidated by kinetic studies, rate law analysis, and deuterium labeling experiments using tiglic acid.[18,26] The reaction begins with

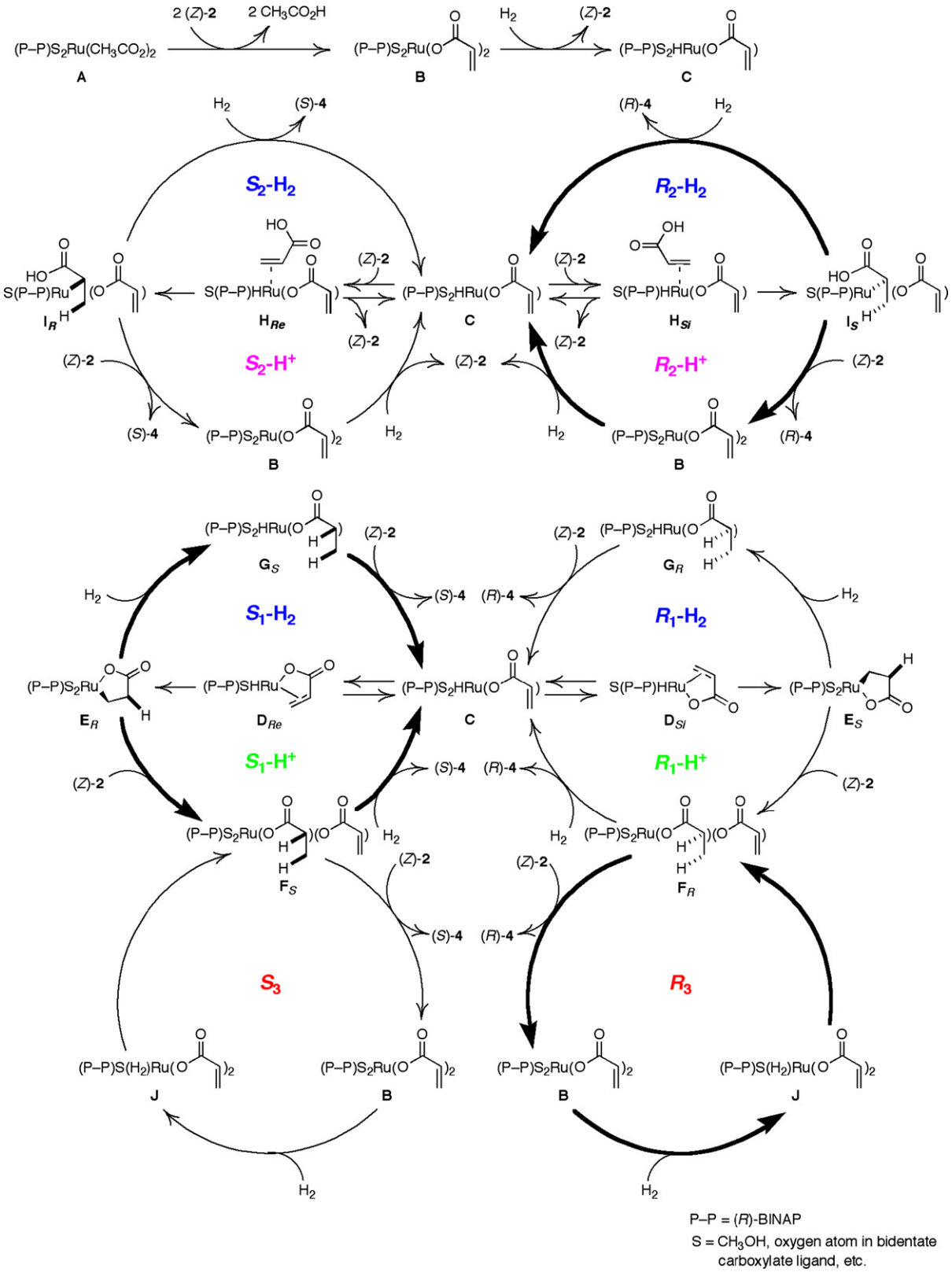

Figure 1. Possible mechanisms for the (*R*)-BINAP–Ru-catalyzed hydrogenation of α,β-unsaturated carboxylic acids in methanol. The C(3)-substituents in the substrates are omitted for clarity. Configuration of the Ru cycles are unspecified.

ligand exchange between the Ru diacetate (*R*)-**1** (**A**) and substrate (*Z*)-**2**, giving (*R*)-**5** (**B**), which causes heterolysis of H_2 to afford catalytic Ru monohydride **C**. This complex is in equilibrium with the chelate olefin complex **D**, which undergoes intramolecular hydride transfer to form the five-membered ring intermediate **E**. Protonolysis of the Ru–C bond with (*Z*)-**2** results in **F**. This step is mediated by methanol. Finally, **F** reacts with H_2 directly or

through **B** formed by **4**/(*Z*)-**2** ligand exchange, giving the Ru hydride **C** and the hydrogenation product **4**, to complete the $\boldsymbol{S_1}$-$\mathbf{H}^+$ and $\boldsymbol{R_1}$-$\mathbf{H}^+$ cycles. This mechanism forms **4**-*h*,*d* with the use of H_2 and CH_3OD. Cycles $\boldsymbol{S_1}$ and $\boldsymbol{R_1}$, giving enantiomeric **4**, are diastereomorphic with one another, and proceed via a series of diastereomeric intermediates. Alternatively, the Ru–C linkage in **E** can be cleaved by H_2 to afford **G**, which, upon ligand exchange with (*Z*)-**2**, completes the $\boldsymbol{S_1}$-$\mathbf{H_2}$ and $\boldsymbol{R_1}$-$\mathbf{H_2}$ cycles. Reaction of **B** or **F** with H_2 limits the overall rate of hydrogenation. This mechanism yields the non-deuterated product **4**-*h*,*h*, even in CH_3OD.

This monohydride mechanism is known to operate in the (*R*)-**1**-catalyzed hydrogenation of enamides,[2,27] in which a RuH/enamide chelate complex undergoes RuH/C=C migratory insertion via a kinetically favored '*exo*' cyclization process. In this reaction, however, the five-membered ring complex **E** formed from **D** requires a spatially constrained '*endo*' addition of the Ru–H linkage to the C(2)=C(3) bond. Therefore, 2+2 Ru–H addition across the olefinic bond occurs also via an additional non-chelate process in which (*Z*)-**2** acts simply as an olefinic substrate.[27] Here the regiochemistry is determined electronically so as to form the more stable Ru–C(2) bond.[28] The resulting **I** is then cleaved either by a proton ($\boldsymbol{S_2}$-$\mathbf{H}^+$ and $\boldsymbol{R_2}$-$\mathbf{H}^+$ cycles) or H_2 ($\boldsymbol{S_2}$-$\mathbf{H_2}$ and $\boldsymbol{R_2}$-$\mathbf{H_2}$ cycles) to give **4**. Each pathway gives **4**-*d*,*h* or **4**-*h*,*h*, respectively. In both $\boldsymbol{S_1}$ and $\boldsymbol{S_2}$ (or $\boldsymbol{R_1}$ and $\boldsymbol{R_2}$) pathways, the two newly incorporated hydrogens have different origins—either H_2 and methanol, or two H_2 molecules.

Furthermore, under certain conditions, the Ru complex can form catalytic Ru 'dihydrides' possessing two hydridic ligands or an η^2-H_2.[29] Hydrogenation of (*Z*)-**2** with such a dihydride ($\boldsymbol{S_3}$ and $\boldsymbol{R_3}$ cycles) produces **4** in which two hydrogen atoms are supplied from a single H_2 molecule. Reaction with H_2 or D_2 gives either **4**-*h*,*h* or **4**-*d*,*d*, respectively, regardless of whether the reaction utilizes deuterated or non-deuterated methanol.

Assuming the possibility of these three cycles, isotopic labeling experiments serve as a useful tool for investigating the pathways leading to the chiral products. When H_2 is replaced by a 1:1 H_2–D_2 mixture, the isotopomers of **4** obtained with H_2 and CH_3OD are redistributed, depending on the relative significance of each of these catalytic cycles. Table 2 shows the theoretical isotopic distribution in each possible catalytic cycle, where the H/D kinetic isotope effects are ignored.

2.4. Pathways leading to varying enantiomers

In asymmetric hydrogenation of unsaturated carboxylic acids, the sense and extent of enantioselectivity as well as the sensitivity to hydrogen pressure are highly dependent upon the substitution pattern of the substrates.[23] Earlier studies on the hydrogenation of tiglic acid in methanol containing (*R*)-**1**, giving *S*-enriched 2-butanoic acid, suggested the operation of the Ru monohydride mechanism, $\boldsymbol{S_1}$-$\mathbf{H}^+$, as the dominant pathway.[18,26,30] However, the details are unknown and, in particular, the origin of the minor *R* enantiomer remains totally unclear. Isotopic labeling experiments provide a key to distinguish the origin of both the enantiomeric products. In addition to the mechanistic models illustrated in Figure 1, there may exist other unknown mechanisms involving different catalytic species. The selectivity *must* be affected by kinetic isotope effects. Nevertheless, comparison of the isotopomer ratios obtained with H_2/CH_3OD and H_2–D_2/CH_3OD allows for the estimation of the relative significance of the three catalytic cycles in the (*R*)-**1**-catalyzed asymmetric hydrogenation of (*Z*)-**2** in methanol.

Table 2. Theoretical isotope distribution factor for 1:1 H_2–D_2 in CH_3OD, assuming no kinetic isotope effect

Entry	Mechanism	**4**-*h*,*h*	**4**-*h*,*d*	**4**-*d*,*h*	**4**-*d*,*d*
1	$\boldsymbol{S_1}$-$\mathbf{H_2}$	0.25	0.25	0.25	0.25
2	$\boldsymbol{S_1}$-$\mathbf{H}^+$	0	0.5	0	0.5
3	$\boldsymbol{S_2}$-$\mathbf{H_2}$	0.25	0.25	0.25	0.25
4	$\boldsymbol{S_2}$-$\mathbf{H}^+$	0	0	0.5	0.5
5	$\boldsymbol{S_3}$	0.5	0	0	0.5

To facilitate the understanding, the results of deuterium labeling experiments in Table 1 are rearranged in Figure 2, particularly focusing on the H_2/CH_3OD and H_2–D_2/CH_3OD systems at 4, 50, and 100 atm. At each hydrogen pressure, the left and right regions correspond to the (*S*)-**4** major product and the minor enantiomeric product (*R*)-**4**. The values shaded in yellow are the observed isotopomer ratios for H_2/CH_3OD (top) and H_2–D_2/CH_3OD (bottom). The detailed process involved in the calculation of the estimated result for H_2–D_2/CH_3OD on the basis of the observed result for H_2/CH_3OD and the theoretical isotopic distribution (Table 2) is shown in the middle unshaded part, in which the isotopomers distributed via the $\boldsymbol{S_1}$-$\mathbf{H}^+$, $\boldsymbol{S_2}$-$\mathbf{H}^+$, $\boldsymbol{S_1}$-$\mathbf{H_2}$ and $\boldsymbol{S_2}$-$\mathbf{H_2}$, and $\boldsymbol{S_3}$ cycles (Fig. 1) are indicated in green, pink, blue, and red, respectively. The colors of the numerical values also correspond to those of the reaction pathways. If the vertical sum of the colored values is consistent with the observed value in the yellow part (bottom), the degree of contribution should be correct. The horizontal sum shows the degree of each catalytic cycle. As accuracy to the tenth place is meaningless in the discussion, all of the calculated values are rounded to the nearest integer. Qualitatively, a marked difference is easily seen both in the *h*,*h*/*h*,*d*/*d*,*h*/*d*,*d* distribution patterns and the patterns of the enantiomeric products, depending on hydrogen pressure and other parameters. Quantification can be performed as follows.

First, the results from the 4 atm reaction are analyzed (Fig. 2a). The hydrogenation generates (*S*)- and (*R*)-**4** in a 97:3 ratio. The major *S* product consists of *h*,*h*, *h*,*d*, *d*,*h*, and *d*,*d* isotopomers in a 10.3:88.7:0.0:1.0 ratio, and the ratio shifts to 3.1:45.9:3.1:47.9 when the conditions are changed to 1:1 H_2–D_2/CH_3OD. The 88.7% *h*,*d* portion can be easily understood as being the product of the $\boldsymbol{S_1}$-$\mathbf{H}^+$ mechanism involving Ru monohydride and a Ru–C(3) species (Fig. 1, middle). $\boldsymbol{S_1}$-$\mathbf{H}^+$ should distribute the 88.7% into the four isotopomers in a 0:0.5:0:0.5 ratio under 1:1 H_2–D_2 conditions (Table 2 entry 2), giving ca. 44 (*S*)-*h*,*d* and ca. 44 (*S*)-*d*,*d*. The 10.3% *h*,*h* portion is expected to be generated via $\boldsymbol{S_1}$-$\mathbf{H_2}$, $\boldsymbol{S_2}$-$\mathbf{H_2}$, and/or $\boldsymbol{S_3}$. With the 1:1 H_2–D_2/CH_3OD system, $\boldsymbol{S_1}$-$\mathbf{H_2}$ and $\boldsymbol{S_2}$-$\mathbf{H_2}$ each give four isotopomers in equal amounts (Table 2, entries 1 and 3), while the $\boldsymbol{S_3}$ route generates them in a 0.5:0:0:0.5 ratio (entry 5). Note that *h*,*h*

(a)

major (*S*)-**4**							minor (*R*)-**4**				
	h,h	*h,d*	*d,h*	*d,d*			*h,h*	*h,d*	*d,h*	*d,d*	
H_2/CH_3OD	10.3	88.7	0.0	1.0	contribution		53.3	30.0	16.7	0.0	H_2/CH_3OD
S_1-H^+		~88.7x0.5		~88.7x0.5	89%	30%		~30.0x0.5		~30.0x0.5	R_1-H^+
S_2-H^+			~0.0x0.5	~0.0x0.5	0%	16%			~16.7x0.5	~16.7x0.5	R_2-H^+
S_1-H_2, S_2-H_2	~10.3x0.25	~10.3x0.25	~10.3x0.25	~10.3x0.25	10%	20%	~20x0.25	~20x0.25	~20x0.25	~20x0.25	R_1-H_2, R_2-H_2
S_3	~0.0x0.5			~0.0x0.5(1)	0%	34%	~34x0.5			~34x0.5	R_3
expected ratio	3	47	3	47			23	20	13	43	expected ratio
H_2–D_2/CH_3OD	3.1	45.9	3.1	47.9			23.3	20.1	13.3	43.3	H_2–D_2/CH_3OD

(b)

major (*S*)-**4**							minor (*R*)-**4**				
	h,h	*h,d*	*d,h*	*d,d*			*h,h*	*h,d*	*d,h*	*d,d*	
H_2/CH_3OD	44.5	52.4	1.0	2.1	contribution		56.7	26.7	16.6	0.0	H_2/CH_3OD
S_1-H^+		~52.4x0.44		~52.4x0.56	52%	26%		~26.7x0.44		~26.7x0.56	R_1-H^+
S_2-H^+			~1.0x0.44	~1.0x0.56	1%	17%			~16.6x0.44	~16.6x0.56	R_2-H^+
S_1-H_2, S_2-H_2	~44.5x0.19	~44.5x0.25	~44.5x0.25	~44.5x0.31	45%	34%	~34x0.19	~34x0.25	~34x0.25	~34x0.31	R_1-H_2, R_2-H_2
S_3	~0.0x0.44			~0.0x0.56(2)	0%	23%	~23x0.44			~23x0.56	R_3
expected ratio	9	35	11.5	44.5			17	20.5	16	46.5	expected ratio
H_2–D_2/CH_3OD	9.3	32.1	11.9	46.7			24.4	15.6	17.8	42.2	H_2–D_2/CH_3OD

(c)

major (*S*)-**4**							minor (*R*)-**4**				
	h,h	*h,d*	*d,h*	*d,d*			*h,h*	*h,d*	*d,h*	*d,d*	
H_2/CH_3OD	57.4	37.8	1.1	3.7	contribution		82.2	9.3	7.8	0.7	H_2/CH_3OD
S_1-H^+		~37.8x0.5		~37.8x0.5	38%	9%		~9.3x0.5		~9.3x0.5	R_1-H^+
S_2-H^+			~1.1x0.5	~1.1x0.5	1%	8%			~7.8x0.5	~7.8x0.5	R_2-H^+
S_1-H_2, S_2-H_2	~57.4x0.25	~57.4x0.25	~57.4x0.25	~57.4x0.25	57%	48%	~48x0.25	~48x0.25	~48x0.25	~48x0.25	R_1-H_2, R_2-H_2
S_3	~0.0x0.5			~0.0x0.5(4)	0%	34%	~34x0.5			~34x0.5(1)	R_3
expected ratio	13	34	13.5	38.5			29	17	16	38	expected ratio
H_2–D_2/CH_3OD	12.8	35.1	11.7	40.4			30.0	16.7	18.3	35.0	H_2–D_2/CH_3OD

Figure 2. Calculation process for obtaining the expected ratios in the 1:1 H_2–D_2/CH_3OD system on the basis of the observed results for the H_2/CH_3OD system. The values shaded in yellow are the observed. The values in parentheses are for some unknown mechanism; (a) 4 atm (*S*)-**4** and (*R*)-**4** were obtained in a 97:3 ratio; (b) 50 atm (*S*)-**4**/(*R*)-**4**=95.5:4.5. A 44:56 H_2–D_2 mixture was used, and this ratio is considered in the calculation of the distribution factors in Table 2; (c) 100 atm (*S*)-**4**/(*R*)-**4**=94:6.

formation occurs in 3.1% yield in the 1:1 H_2–D_2/CH_3OD system. Where the entire 10.3 parts to be split equally among *h,h*, *h,d*, *d,h*, and *d,d*, the yield would be 2.6%, which is within the expanded range of experimental error expected if the S_3 mechanism is involved.

The *d,h* isotopomer, which should originate from the S_2-H^+ cycle via Ru–H and the Ru–C(2) species (Fig. 2a), can be divided into *d,h* and *d,d* in the 1:1 H_2–D_2/CH_3OD system. As there is no *d,h* formed in the 4-atm experiment for the major product, the *d,h* and *d,d* are also 0 under H_2–D_2 conditions. The sum of the colored values in a column gives 3:47:3:47, which is highly consistent with the observed ratio of 3.1:45.9:3.1:47.9. The origin of the 1.0 part of *d,d* is not clear.[31] Thus, the contribution of S_1-H^+ and S_1-H_2/S_2-H_2 in the formation of (*S*)-**4** is ca. 89% and 10%, respectively.

The minor product (*R*)-**4** produces totally different patterns from those of the major product (Fig. 2a, right). The observed ratio of *h,h*, *h,d*, *d,h*, and *d,d* is 53.3:30.0:16.7:0.0, which is characterized by a large amount of *h,h*. Gaseous hydrogen is more utilized in comparison with the major (*S*)-**4** case. This phenomenon can be explained by the involvement of the R_3 cycle via a RuH_2 species and the R_2-H_2 cycle via RuH and Ru-C(2) species (Fig. 1, bottom and top). A change to 1:1 H_2–D_2/CH_3OD gives a 23.3:20.1:13.3:43.3 mixture. Thus, taking the 23.3 parts *h,d* into consideration, ca. 20 of the 53.3 parts from the H_2/CH_3OD system can be distributed equally among *h,h*, *h,d*, *d,h*, and *d,d* (5:5:5:5) via the R_1-H_2 cycle, and the remaining ca. 34 to *h,h* and *d,d* (17:17) via a RuH_2-involved R_3 route. The 30 parts of *h,d* generated by R_1-H^+ are divided equally between *h,d* and *d,d*, and the 16.7 parts *d,h* generated via R_2-H^+ are divided equally between *d,h* and *d,d*. The vertical sum of these colored values gives a ca. 23:20:13:43 ratio, which is, again, quite consistent with the observed ratio. These results indicate that 34%, 46%, and 20% of the minor product (*R*)-**4** is generated via a RuH_2 route (R_3), a RuH-protonolysis route (R_2-H^+ and/or R_1-H^+), and a RuH-hydrogenolysis route (R_1-H_2 and/or R_2-H_2), respectively.

Good agreement between the values estimated from the H_2/CH_3OD results and the experimentally observed values can be seen both in the major and minor cases, even with changes in hydrogen pressure and the H_2–D_2 ratio (Fig. 2b and c). In all cases, an increase in the H_2 pressure from 4 to 50 atm and then to 100 atm in CH_3OD enhances the contribution of gaseous hydrogen, giving larger amount of the *h,h* isotopomers (major: 10.3→44.5→57.4; minor: 53.3→56.7→82.2) together with a significant decrease in the *h,d* isotopomers (major: 88.7→52.4→37.8; minor: 30.0→26.7→9.3). A similar detailed analysis of the 50 atm H_2–D_2/CH_3OD results reveals that the major *S* product formed by RuH involves the S_1-H_2/S_2-H_2 cycle (45%) and S_1-H^+ cycle (52%), and that the involvement of S_2-H^+ and S_3 is negligible (Fig. 2b). On the other hand, ca. 40% of the *R*

minor product is formed via R_2-H^+ (17%) and R_3 (23%) cycles. The same tendency is observed with the 100 atm H_2–D_2/CH_3OD system (Fig. 2c): S_1-H_2/S_2-H_2, 57%; S_1-H^+, 38%; S_2-H^+, 1%; S_3, 0% versus R_1-H_2/R_2-H_2, 48%; R_1-H^+, 9%; R_2-H^+, 8%; R_3, 34%. Although the R_1-H_2/R_2-H_2 ratio cannot be determined by the present isotope labeling method, a significant contribution from R_2-H_2 is expected in the formation of the *R* minor product by taking the R_2-H^+/R_1-H^+ ratio (ca. 1:1) into consideration.

These results indicate that the chelate RuH cycles S_1 and R_1 is *S* selective, but the non-chelate RuH cycles S_2 and R_2 and the RuH_2 cycles S_3 and R_3 are *R*-selective. Thus, the pathway forming the minor enantiomer is complicated and is not straightforward, while the major enantiomer is produced primarily (99% at 4 atm and 95% at 100 atm) by the standard monohydride mechanism.

3. Conclusion

Asymmetric catalysis converts a prochiral substrate into an enantiomerically-enriched chiral product. The enantioselectivity has generally been interpreted as a result of competing diastereomorphic catalytic cycles involving a single chiral catalyst without substantiation of the presupposition of the existence of the competing cycles. This BINAP–Ru-catalyzed asymmetric hydrogenation of an α,β-unsaturated carboxylic acid, together with earlier examples[18,26] suggests caution in making such an interpretation. This study indicates that: (1) the hydrogenation can involve several catalytic species, and (2) the major and minor enantiomers can be produced by different pathways.

4. Experimental

4.1. General

Nuclear magnetic resonance (NMR) spectra were measured on either a JEOL JNM-A400 equipped with a pulsed field gradient unit and a triple-resonance probe, a JEOL JNM-ECP500, or a Varian INOVA-500 instrument. The chemical shifts are expressed either in parts per million (ppm) downfield from $Si(CH_3)_4$ or in ppm relative to $CHCl_3$ (δ 7.26 in ^1H NMR and δ 77.0 in ^{13}C NMR). Signal patterns of ^1H NMR as well as ^{13}C NMR are indicated as s, singlet; d, doublet; t, triplet; q, quartet; m, multiplet; br, broad signal. GC–MS analyses were performed using a Shimadzu QP-5000. All melting points were determined with a Yanaco melting point apparatus and are uncorrected.

Analytical thin layer chromatography (TLC) was performed using Merck 5715 indicating plates precoated with silica gel 60 F_{254} (layer thickness: 0.25 mm). Liquid chromatographic purifications were performed by flash column chromatography, using glass columns packed with Merck 9385 (230–400 mesh). For analytical and preparative HPLC, a Shimadzu LC-10AD instrument equipped with a SCL-10A system controller, a DGU-4A degasser, a SIL-10AXL autosampler, a GILSON MODEL 201 fraction collector, and a Shimadzu SPD-10A UV detector were used. A DAICEL CHIRALCEL OD packed with cellulose tris(3,5-dimethylphenylcarbamate) was used as a column. Eluted compounds were detected at 254 nm.

All manipulations in the BINAP–Ru-catalyzed hydrogenation were carried out using a standard Schlenk technique on a dual manifold vacuum/Ar system. The structures of (*Z*)-**2** and (*E*)-**2** were determined by comparing the spectral data with reported values.[32] Conversion of (*Z*)-**2** and (*E*)-**2** was evaluated by comparison of the ^1H NMR signal intensity ratio at δ 2.18 (CH_3 of (*Z*)-**2**), δ 2.61 (CH_3 of (*E*)-**2**), and δ 1.31 (CH_3 of **4**). The ee values of **4** were determined by HPLC analysis (conditions: column, CHIRALCEL OD (10 mm×25 cm); eluent, a 1000:1:3 mixture of hexane/2-propanol/acetic acid; flow rate, 3 mL min^{-1}; temperature, 30 °C; detector, 254 nm; retention time (t_R) of (*R*)-**4**, 27 min; t_R of (*S*)-**4**, 43 min) The absolute configuration of the hydrogenation product **4** was determined by comparison of the sign of the optical rotation with the reported value.[33]

4.2. Materials

CH_3OH and CH_3OD for hydrogenation were degassed at reflux in the presence of Mg (250 mg/100 mL) under argon for 6 h and distilled into Schlenk flasks. CH_3OD contains 0.5% OH species. The solvent was further degassed by three freeze–thaw cycles before hydrogenation. $CDCl_3$ and D_2O were purchased from Aldrich Chemical Co. and used without further purification.

Ar gas was purified by passing it through a column of BASF R3-11 catalyst at 80 °C, and then through a column of $CaSO_4$ at room temperature. H_2 gas of 99.99999% purity and D_2 gas containing 0.4% HD were purchased from Nippon Sanso, and HD gas containing 2% H_2 and 2% D_2 was obtained from Isotec. These gases were used for hydrogenation without purification. A 1:1 mixture of H_2 and D_2 gases was prepared by mixing 50 atm H_2 and 50 atm D_2 at −20 °C in a stainless steel autoclave containing a glass vessel. The H_2/HD/D_2 ratio was determined by GC analysis. Ne and He for GC analysis of the H_2/HD/D_2 ratio were obtained from Takachiho Kogyo and the Japan Helium Center, respectively. He gas, purchased from Nippon Sanso, was used for GC–MS analysis of the CH_3OH/CH_3OD ratio. The purities of Ne and He were 99.999% and 99.9999%.

$Ru(CH_3COO)_2$[(*R*)-binap] [(*R*)-**1**] and $Ru(CH_3COO)_2$[(*S*)-binap] [(*S*)-**1**] were prepared by the literature method.[17b] (*Z*)-3-Phenyl-2-butenoic acid [(*Z*)-**2**] (mp 129.6–130.8 °C) was synthesized according to the known method.[32] The D-labeled substrates (*Z*)-**2**-2-*d* and (*E*)-**2**-2-*d* were synthesized by addition of $(CH_3)_2CuLi$ to phenylpropionic acid, followed by treatment with 1 N DCl in D_2O solution, in a way similar to the established procedure for synthesis of the nonlabeled compound[32] (mp=130.6–131.8 °C for (*Z*)-**2**-2-*d* and 95.0–95.7 °C for (*E*)-**2**-2-*d*). The ^{13}C-labeled substrate, (*Z*)-**2**-3-^{13}C, was prepared from trimethyl phosphonoacetate and acetophenone-*carbonyl*-^{13}C according to the literature method for preparation of the unlabeled compound.[34] The substrate

was purified by recrystallization from 3:1 hexane/ether at 4 °C (mp 129.0–131.0 °C).

4.3. Asymmetric hydrogenation of (*Z*)-3-phenyl-2-butenoic acid [(*Z*)-2]

The experiment with H_2/CH_3OH was conducted in an 80-mL Schlenk tube equipped with a Young's tap for the 1-atm trial, and in an 80-mL glass autoclave for the 4-atm trial. The high-pressure reaction was carried out in an 80-mL glass vessel placed in a stainless steel autoclave.

H_2/CH_3OH (1 atm): the substrate, (*Z*)-**2** (58.2 mg, 0.36 mmol), and CH_3OH (3.6 mL) were placed into a dry, Ar-filled, 20-mL Schlenk tube. The solution was degassed by three freeze–thaw cycles, and was transferred via a stainless canula to another 20-mL Schlenk tube containing (*R*)-**1** (1.5 mg, 1.8 μmol). After the resulting yellow solution of the substrate and catalyst was degassed by two freeze–thaw cycles, it was introduced into the Ar-filled reaction vessel and then stirred under an initial H_2 pressure of 1 atm at 30 °C for 116 h. After removal of the solvent, conversion of (*Z*)-**2** was determined by ^1H NMR analysis to be 100%. The crude reaction mixture was purified on a silica gel column (eluent, 1:1 hexane/ether) to give (*S*)-**4** in 94% ee.

H_2/CH_3OH (4 atm): 59.3 mg (100 mM) (*Z*)-**2**, [(*R*)-**1**]=0.5 mM; 4 atm H_2; CH_3OH; 30 °C; 48 h. The conversion and ee were 100% and 94%, respectively.

H_2/CH_3OH (50 atm): 99.2 mg (100 mM) (*Z*)-**2**, [(*R*)-**1**]=0.5 mM; 50 atm H_2; CH_3OH; 30 °C; 24 h. The conversion and ee were 100% and 92%, respectively.

H_2/CH_3OH (100 atm): 99.4 mg (100 mM) (*Z*)-**2**, [(*R*)-**1**]=0.5 mM; 100 atm H_2; CH_3OH; 30 °C; 12 h. The conversion and ee were 100% and 88%, respectively. (*S*)-**4**: ^1H NMR (400 MHz, $CDCl_3$) δ 1.31 (d, 3, J=6.8 Hz, CH_3), 2.57 (dd, 1, J=16 Hz and 8.3 Hz, C(2)H_S), 2.66 (dd, 1, J=16 and 6.8 Hz, C(2)H_R), 3.26 (ddd, 1, J=8.3, 6.8 and 6.8 Hz, C(3)H), 7.17–7.32 (m, 5, aromatic), 9.40–10.50 (br, 1, COOH).

4.4. X-ray crystallographic analyses for Ru[(*Z*)-$CH_3(C_6H_5)$C=CHCOO]$_2$[(*R*)-binap]

Ru($CH_3COO)_2$[(*R*)-binap] [(*R*)-**1**] (50.6 mg, 60.1 μmol) and (*Z*)-**2** (208 mg, 1.28 mmol) were placed in a dry 20-mL Schlenk tube, and CH_3OH (15 mL) was introduced under an Ar stream. The solution was stirred for 1 h at room temperature, during which time a yellow solid precipitated. The supernatant liquid was removed via a canula covered with filter paper at one end. The solid was washed with CH_3OH (10 mL) and dried in vacuo, affording yellow powdery crystals of Ru[(*Z*)-$CH_3(C_6H_5)$C=CHCOO]$_2$[(*R*)-binap] [(*R*)-**5**] (32.6 mg, 52% yield). Orange prismatic crystals were obtained by recrystallization of (*R*)-**5** (ca. 10 mg) using a liquid–liquid diffusion of hexane (4 mL) into toluene (1 mL) at 4 °C. A single crystal (0.22 mm×0.20 mm×0.14 mm) was mounted on the top of a quartz fiber with a small amount of epoxy resin adhesive and transferred to a goniometer head. The data was collected in a −100 °C nitrogen atmosphere. The molecular structure of (*R*)-**5** is illustrated in Figure 3.

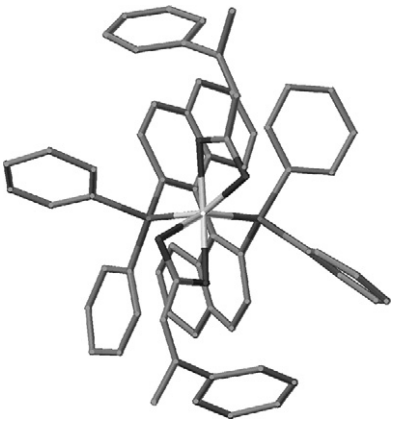

Figure 3. The X-ray crystal structure of Ru[(*Z*)-$CH_3(C_6H_5)$C=CHCOO]$_2$[(*R*)-bianp] [(*R*)-**5**].

4.5. Isotopic labeling experiments

4.5.1. H_2/HD/D_2 and CH_3OH/CH_3OD analysis. The H_2/HD/D_2 ratio was analyzed via low temperature column chromatography according to published methods.[2,35] The CH_3OH/CH_3OD ratio was determined by GC–MS analysis on a Shimadzu GCMS-QP5000.[2]

4.5.2. Structural determination of isotopomers. The structures of the four isotopomers, **4**-*h*,*h*, **4**-*h*,*d*, **4**-*d*,*h*, and **4**-*d*,*d*, were determined by analyses of the $^{13}C\{^1H\}$ NMR spectra and $^{13}C\{^1H,^2H\}$–^1H correlation spectra taken in $CDCl_3$ at 23 °C using a JEOL JNM-A400. To minimize the magnetic field instability associated with no D-spin lock, the measuring time was shortened by use of a high concentration of the sample (69 mg/0.6 mL), an acquisition time of 0.550 s, a pulse delay of 2.000 s, a scan number of 16, and a measurement time of 95 min. The α-carbons of the four isotopomers resonate at δ 42.58, 42.48, 42.26, and 42.16 as singlets and were correlated with the α-proton signals at δ 2.665 (dd, J=7 and 15 Hz) and 2.567 (dd, J=7 and 15 Hz), 2.656 (d, J=15 Hz) and 2.560 (d, J=15 Hz), 2.640 (d, J=9 Hz), and 2.641 (s), respectively. From analysis of the coupling mode, the four α-carbon signals from low to high field were assigned to **4**-*h*,*h*, **4**-*h*,*d*, **4**-*d*,*h*, and **4**-*d*,*d*. In a similar way, the C(3) carbon signals at δ 36.10, 36.04, 35.71, and 35.65 were assigned to **4**-*h*,*h*, **4**-*d*,*h*, **4**-*h*,*d*, and **4**-*d*,*d*, respectively. These assignments were consistent with the empirical rule that a D-possessing carbon atom resonates at higher field with a larger number of D.[36] (*S*)-**4**: ^1H NMR (400 MHz, $CDCl_3$) δ 2.560 (d, J=15 Hz, C(2)H_S of **4**-*h*,*d*), 2.567 (dd, J=7 and 15 Hz, C(2)H_S of **4**-*h*,*h*), 2.640 (d, J=9 Hz, C(2)H of **4**-*d*,*h*), 2.641 (s, C(2)H of **4**-*d*,*d*), 2.656 (d, J=15 Hz, C(2)H_R of **4**-*h*,*d*), 2.665 (dd, J=7 and 15 Hz, C(2)H_R of **4**-*h*,*h*). $^{13}C\{^1H,^2H\}$ NMR (100 MHz, $CDCl_3$) δ 35.65 (s, C(3) of **4**-*d*,*d*), 35.71 (s, C(3) of **4**-*h*,*d*), 36.04 (s, C(3) of **4**-*h*,*d*), 36.10 (s, C(3) of **4**-*d*,*h*), 42.16 (s, C(2) of **4**-*d*,*d*), 42.26 (s, C(2) of **4**-*d*,*h*), 42.48 (s, C(2) of **4**-*h*,*d*), 42.58 (s, C(2) of **4**-*h*,*h*). $^{13}C\{^1H\}$ NMR (100 MHz, $CDCl_3$) δ 35.65 (t, J= 21 Hz, C(3) of **4**-*d*,*d*), 35.71 (t, J=20 Hz, C(3) of **4**-*h*,*d*), 36.04 (s, C(3) of **4**-*d*,*h*), 36.10 (s, C(3) of **4**-*h*,*h*), 42.16 (t, J=19 Hz, C(2) of **4**-*d*,*d*),

42.26 (t, J=19 Hz, C(2) of **4**-*d*,*h*), 42.48 (s, C(2) of **4**-*h*,*d*), 42.58 (s, C(2) of **4**-*h*,*h*).

4.5.3. Determination of the relative stereochemistry of 4-*d*,*h*. The relative stereochemistry of **4**-*d*,*h* was determined by comparing the ^{1}H NMR data with those of reference isotopomers, namely a mixture of (2*R**,3*S**)-**4**-*d*,*h* and (2*S**,3*S**)-**4**-*d*,*h* prepared by reduction of (*Z*)-**2**-2-*d* and (*E*)-**2**-2-*d*, respectively, with diimide (Section 4.5.4), which is known to proceed via cis addition of hydrogen.[21] ^{1}H NMR of (2*R**,3*S**)-**4**-*d*,*h* (500 MHz, $CDCl_3$) δ 2.53 (1, br d, J=8.3 Hz, C(2)H). ^{1}H NMR of (2*S**,3*S**)-**4**-*d*,*h* (500 MHz, $CDCl_3$) δ 2.64 (1, dr s, C(2)H). Because of the priority rule, (2*R*,3*S*)-**4**-*d*,*h*-3-^{13}C and (2*S*,3*R*)-**4**-*d*,*h*-3-^{13}C correspond to (2*S**,3*S**)-**4**-*d*,*h*.

4.5.4. Synthesis of reference isotopomers. The 3*S*-enriched reference isotopomers **4**-*h*,*h*, **4**-*d*,*d* and mixtures of **4**-*h*,*h* and **4**-*h*,*d*, and **4**-*d*,*h* and **4**-*d*,*d* were prepared by the reduction of (*Z*)-**2** under the following conditions. For **4**-*h*,*h*: (*Z*)-**2** (50.0 mg, 0.31 mmol); (*S*)-**1** (1.0 mg, 1.2 μmol); CH_3OH (3.1 mL); 4 atm H_2; 30 °C; 48 h. For **4**-*d*,*d*: (*Z*)-**2** (50.0 mg, 0.31 mmol); (*S*)-**1** (1.0 mg, 1.2 μmol); CH_3OD (3.1 mL); 1 atm D_2; 30 °C; 216 h. For a 77:23 mixture of **4**-*h*,*h* and **4**-*d*,*h*: (*Z*)-**2** (100 mg, 0.62 mmol); (*S*)-**1** (3.0 mg, 3.6 μmol); CH_3OD (6.2 mL); 4 atm HD; 30 °C; 338 h. For a 24:76 mixture of **4**-*h*,*d* and **4**-*d*,*d*: (*Z*)-**2** (100 mg, 0.62 mmol); (*S*)-**1** (3.0 mg, 3.6 μmol); CH_3OD (6.2 mL); 4 atm HD; 30 °C; 168 h. All conversions were 100%. Products were purified by silica gel column chromatography (eluent, 1:1 hexane/ether).

The reference isotopomers (2*R**,3*S**)-**4**-*d*,*h* and (2*S**,3*S**)-**4**-*d*,*h* were prepared by the reduction of (*Z*)-**2**-2-*d* and (*E*)-**2**-2-*d* with diimide under the following conditions. (2*R**,3*S**)-**4**-*d*,*h*: (*Z*)-**2**-2-*d* (22.0 mg, 0.14 mmol); $NH_2NH_2\cdot H_2O$ (40 mg, 0.80 mmol); $CuSO_4\cdot 5H_2O$ (1.4 mg, 5.6 μmol); C_2H_5OH (3.0 mL); 22 h; 10% conversion. For (2*S**,3*S**)-**4**-*d*,*h*: (*E*)-**2**-2-*d* (22.0 mg, 0.14 mmol); $NH_2NH_2\cdot H_2O$ (40 mg, 0.80 mmol); $CuSO_4\cdot 5H_2O$ (1.4 mg, 5.6 μmol); C_2H_5OH (3.0 mL); 22 h; 35% conversion. No *E*/*Z* isomerization was observed in the reduction of (*E*)-**2**-2-*d*, whereas the unreacted substrate contained about 10% of the *E* isomer in the reduction of (*Z*)-**2**-2-*d*.

4.5.5. Separation of the enantiomers. The major (*S*)-**4** and minor (*R*)-**4** products obtained in the BINAP–Ru-catalyzed hydrogenation with either H_2/CH_3OD, H_2–D_2/CH_3OD, or D_2/CH_3OD were separated under the following conditions: a mixture of (*Z*)-**2** and **4**, 20–25 mg; column, CHIRALCEL OD (20 mm×250 mm); eluent, 1000:1:3 hexane/2-propanol/acetic acid; flow rate, 10.0 mL min^{-1}; temperature, 30 °C; detector, 254 nm; t_R of (*R*)-**4**, 45 min; t_R of (*S*)-**4**, 85 min. There is no overlap of the compounds.

4.5.6. Determination of the isotopomer ratios. The isotopomer ratios of (*S*)-**4**-3-^{13}C and (*R*)-**4**-3-^{13}C were determined by measurement of the C(3) carbon signal area in the $^{13}C\{^1H,^2H\}$ NMR spectra, which were taken using a nanoprobe under the following conditions: flip angle, 48.0 °; acquisition time (AT), 2.621 s; pulse delay (PD), 30.000 s; sample concentration, 1.0 mg/40 μL; measurement time, 256 scans (2.3 h). ^{1}H and ^{2}H decoupling was effected only during the acquisition time. The values of relaxation time, T_1, obtained by the inversion recovery method were <4.5 s for both C(2) and C(3) carbons and <5 s for all protons. These values satisfied the necessary conditions, PD>5×T_1 for protons and AT+PD> 5×T_1 for carbons.

4.5.7. H_2/CH_3OD conditions. The experiments with H_2/CH_3OD under 4 or 10 atm were conducted in a 400-mL glass autoclave, whereas the high-pressure reactions under 50 or 100 atm of H_2 were carried out in a 200-mL glass vessel placed in a stainless steel autoclave.

H_2/CH_3OD (4 atm): reaction scale, 202 mg (100 mM) (*Z*)-**2**-3-^{13}C; [(*R*)-**1**]=0.5 mM; 4 atm H_2; CH_3OD; 30 °C. After 9 h, the gas in the reaction vessel was transferred to an 80-mL vacuumed Schlenk flask, and the solvent was recovered by distillation. The $H_2/HD/D_2$ and CH_3OH/CH_3OD ratios, as analyzed by the methods above, were 98.0:2.0:0 and <1:>99, respectively. The residue was subjected to ^{1}H NMR and HPLC analyses, which determined the conversion and ee to be 10% and 94%, respectively. The crude reaction mixture was purified by silica gel column chromatography (eluent, 1:1 hexane/ether) to remove the Ru complex. The (*Z*)-**2**-3-^{13}C and **4**-3-^{13}C mixture was separated by preparative HPLC (conditions, see Section 4.5.5) to give (*Z*)-**2**-3-^{13}C, (*S*)-**4**-3-^{13}C containing (*S*)-**4**-*h*,*h*-3-^{13}C, (*S*)-**4**-*h*,*d*-3-^{13}C, (2*R*,3*S*)-**4**-*d*,*h*-3-^{13}C, and (2*R*,3*S*)-**4**-*d*,*d*-3-^{13}C in a 10.3:88.7:0.0:1.0 ratio and (*R*)-**4**-3-^{13}C containing (*R*)-**4**-*h*,*h*-3-^{13}C, (*R*)-**4**-*h*,*d*-3-^{13}C, (2*S*,3*R*)-**4**-*d*,*h*-3-^{13}C, and (2*S*,3*R*)-**4**-*d*,*d*-3-^{13}C, in a 53.3:30.0:16.7:0.0 ratio. The ratio of the ^{1}H NMR signal intensity at δ 2.62–2.71(m) and δ 2.53–2.62(m) was 100:99 for the major enantiomer and 100:83 for the minor enantiomer.

H_2/CH_3OD (10 atm): reaction scale, 202 mg (100 mM) (*Z*)-**2**-3-^{13}C; [(*R*)-**1**]=0.5 mM; 10 atm H_2; CH_3OD; 30 °C; 10 h. These conditions converted 10% of the (*Z*)-**2**-3-^{13}C to give (*S*)-**4**-3-^{13}C in 94% ee. The $H_2/HD/D_2$ and CH_3OH/CH_3OD ratios were 98.7:1.3:0 and <1:>99. The (*S*)-**4**-*h*,*h*-3-^{13}C/(*S*)-**4**-*h*,*d*-3-^{13}C/(2*R*,3*S*)-**4**-*d*,*h*-3-^{13}C/(2*R*,3*S*)-**4**-*d*,*d*-3-^{13}C ratio and the (*R*)-**4**-*h*,*h*-3-^{13}C/(*R*)-**4**-*h*,*d*-3-^{13}C/(2*S*,3*R*)-**4**-*d*,*h*-3-^{13}C/(2*S*,3*R*)-**4**-*d*,*d*-3-^{13}C ratio were 22.7:75.8:0.5:1.0 and 56.7:26.7:16.6:0.0. The ratio of the ^{1}H NMR signal intensity at δ 2.62–2.71(m) and δ 2.53–2.62(m) was 100:98 for the major enantiomer and 100:83 for the minor enantiomer.

H_2/CH_3OD (50 atm): reaction scale, 202 mg (100 mM) (*Z*)-**2**-3-^{13}C; [(*R*)-**1**]=0.5 mM; 50 atm H_2; CH_3OD; 30 °C; 10 min. These conditions converted 16% of the (*Z*)-**2**-3-^{13}C to give (*S*)-**4**-3-^{13}C in 91% ee. The $H_2/HD/D_2$ and CH_3OH/CH_3OD ratios were 99.7:0.3:0 and <1:>99. The (*S*)-**4**-*h*,*h*-3-^{13}C/(*S*)-**4**-*h*,*d*-3-^{13}C/(2*R*,3*S*)-**4**-*d*,*h*-3-^{13}C/(2*R*,3*S*)-**4**-*d*,*d*-3-^{13}C ratio and the (*R*)-**4**-*h*,*h*-3-^{13}C/(*R*)-**4**-*h*,*d*-3-^{13}C/(2*S*,3*R*)-**4**-*d*,*h*-3-^{13}C/(2*S*,3*R*)-**4**-*d*,*d*-3-^{13}C ratio were 44.5:52.4:1.0:2.1 and 72.9:15.5:11.1:0.5. The ratio of the ^{1}H NMR signal intensity at δ 2.62–2.71(m) and δ 2.53–2.62(m) was 100:98 for the major enantiomer and 100:89 for the minor enantiomer.

H_2/CH_3OD (100 atm): reaction scale, 202 mg (110 mM) (*Z*)-**2**-3-^{13}C; [(*R*)-**1**]=0.5 mM; 100 atm H_2; CH_3OD; 30 °C; 7 min. These conditions converted 22% of the (*Z*)-**2**-3-^{13}C

to give (*S*)-**4**-3-^{13}C in 88% ee. The H_2/HD/D_2 and CH_3OH/CH_3OD ratios were 99.8:0.2:0 and <1:>99. The (*S*)-**4**-*h*,*h*-3-^{13}C/(*S*)-**4**-*h*,*d*-3-^{13}C/(2*R*,3*S*)-**4**-*d*,*h*-3-^{13}C/(2*R*,3*S*)-**4**-*d*,*d*-3-^{13}C ratio and the (*R*)-**4**-*h*,*h*-3-^{13}C/(*R*)-**4**-*h*,*d*-3-^{13}C/(2*S*,3*R*)-**4**-*d*,*h*-3-^{13}C/(2*S*,3*R*)-**4**-*d*,*d*-3-^{13}C ratio were 57.4:37.8:1.1:3.7 and 82.2:9.3:7.8:0.7. The ratio of the ^{1}H NMR signal intensity at δ 2.62–2.71(m) and δ 2.53–2.62(m) was 100:95 for the major enantiomer and 100:92 for the minor enantiomer. Under all conditions, the ratio of the ^{1}H NMR signal intensities were quite consistent with the values calculated from the ^{13}C signal intensities, and the C(2)H/C(3)CH_3 proton signal ratio of the recovered (*Z*)-**2**-3-^{13}C were determined to be 1.0:3.0 by ^{1}H NMR analysis (flip angle, 45°; repetition time, 10 s; measurement time, 128 scans).

4.5.8. H_2–D_2/CH_3OD conditions. The procedure for the H_2–D_2/CH_3OD system was the same as that for the H_2/CH_3OD system.

H_2–D_2/CH_3OD (4 atm): reaction scale, 202 mg (100 mM) (*Z*)-**2**-3-^{13}C; [(*R*)-**1**]=0.5 mM; 4 atm H_2–D_2; CH_3OD; 30 °C; 9 h. These conditions converted 17% of the (*Z*)-**2**-3-^{13}C to give (*S*)-**4**-3-^{13}C in 94% ee. The H_2/HD/D_2 and CH_3OH/CH_3OD ratios were 49.0:2.3:48.7 and <1:>99. The (*S*)-**4**-*h*,*h*-3-^{13}C/(*S*)-**4**-*h*,*d*-3-^{13}C/(2*R*,3*S*)-**4**-*d*,*h*-3-^{13}C/(2*R*,3*S*)-**4**-*d*,*d*-3-^{13}C ratio and the (*R*)-**4**-*h*,*h*-3-^{13}C/(*R*)-**4**-*h*,*d*-3-^{13}C/(2*S*,3*R*)-**4**-*d*,*h*-3-^{13}C/(2*S*,3*R*)-**4**-*d*,*d*-3-^{13}C ratio were 3.1:45.9:3.1:47.9 and 23.3:20.1:13.3:43.3. The intensity ratios of the ^{1}H NMR signals at δ 2.62–2.71(m) and δ 2.53–2.62(m) were 100:48 for the major enantiomer and 100:43 for the minor enantiomer, respectively.

H_2–D_2/CH_3OD (50 atm): reaction scale, 202 mg (100 mM) (*Z*)-**2**-3-^{13}C; [(*R*)-**1**]=0.5 mM; 50 atm H_2–D_2; CH_3OD; 30 °C; 12 min. These conditions converted 10% of (*Z*)-**2**-3-^{13}C to give (*S*)-**3**-3-^{13}C in 92% ee. The H_2/HD/D_2 and CH_3OH/CH_3OD ratios were 44.0:0.3:55.7 and <1:>99. The (*S*)-**4**-*h*,*h*-3-^{13}C/(*S*)-**4**-*h*,*d*-3-^{13}C/(2*R*,3*S*)-**4**-*d*,*h*-3-^{13}C/(2*R*,3*S*)-**4**-*d*,*d*-3-^{13}C ratio and the (*R*)-**4**-*h*,*h*-3-^{13}C/(*R*)-**4**-*h*,*d*-3-^{13}C/(2*S*,3*R*)-**4**-*d*,*h*-3-^{13}C/(2*S*,3*R*)-**4**-*d*,*d*-3-^{13}C ratio were 9.3:32.1:11.9:46.7 and 24.4:15.6:17.8:42.2. The ratio of the ^{1}H NMR signal intensity at δ 2.62–2.71(m) and δ 2.53–2.62(m) was 100:40 for the major enantiomer and 100:38 for the minor enantiomer.

H_2–D_2/CH_3OD (100 atm): reaction scale, 202 mg (100 mM) (*Z*)-**2**-3-^{13}C; [(*R*)-**1**]=0.5 mM; 100 atm H_2–D_2; CH_3OD; 30 °C; 7 min. These conditions converted 6% of (*Z*)-**2**-3-^{13}C to give (*S*)-**4**-3-^{13}C in 88% ee. The H_2/HD/D_2 and CH_3OH/CH_3OD ratios were 48.6:2.0:49.4 and <1:>99. The (*S*)-**4**-*h*,*h*-3-^{13}C/(*S*)-**4**-*h*,*d*-3-^{13}C/(2*R*,3*S*)-**4**-*d*,*h*-3-^{13}C/(2*R*,3*S*)-**4**-*d*,*d*-3-^{13}C ratio and the (*R*)-**4**-*h*,*h*-3-^{13}C/(*R*)-**4**-*h*,*d*-3-^{13}C/(2*S*,3*R*)-**4**-*d*,*h*-3-^{13}C/(2*S*,3*R*)-**4**-*d*,*d*-3-^{13}C ratio were 12.8:35.1:11.7:40.4 and 30.0:16.7:18.3:35.0. The ratio of the ^{1}H NMR signal intensity at δ 2.62–2.71(m) and δ 2.53–2.62(m) was 100:45 for the major enantiomer and 100:45 for the minor enantiomer. At all conditions, the proton signal ratio of the vinylic proton and the CH_3 of the recovered (*Z*)-**2**-3-^{13}C was determined to be 1.0:3.0 by ^{1}H NMR analysis.

4.5.9. D_2/CH_3OD condition. The procedure was the same as that for the H_2/CH_3OD system except for the size of the reactor (250-mL Schlenk tube) and the purification process. D_2/CH_3OD (4 atm): reaction scale, 123 mg (100 mM) (*Z*)-**2**-3-^{13}C; [(*R*)-**1**]=0.5 mM; 4 atm D_2; CH_3OD; 30 °C; 35.2 h. These conditions converted 99.9% of (*Z*)-**2**-3-^{13}C to give (*S*)-**4**-3-^{13}C in 94% ee. The H_2/HD/D_2 and CH_3OH/CH_3OD ratios were 0:2.0:98.0 and 1:99. The (*S*)-**4**-*h*,*h*-3-^{13}C/(*S*)-**4**-*h*,*d*-3-^{13}C/(2*R*,3*S*)-**4**-*d*,*h*-3-^{13}C/(2*R*,3*S*)-**4**-*d*,*d*-3-^{13}C ratio and the (*R*)-**4**-*h*,*h*-3-^{13}C/(*R*)-**4**-*h*,*d*-3-^{13}C/(2*S*,3*R*)-**4**-*d*,*h*-3-^{13}C/(2*S*,3*R*)-**4**-*d*,*d*-3-^{13}C ratio were 0:0:1.1:98.9 and 0:0:0:>99.9. The proton signal ratio of the vinylic proton and the CH_3 of the recovered (*Z*)-**2**-3-^{13}C was determined to be 1.0:3.0 by ^{1}H NMR analysis.

4.5.10. Isotope stability of (2*R*,3*R*)-4-*d*,*d*. The hydrogenation of tiglic acid (13.7 mg, 0.137 mmol) was carried out in CH_3OH (2.7 mL) containing (2*R*,3*R*)-**4**-*d*,*d* with an ee of 94% (22.3 mg, 0.137 mmol) under 4 atm of H_2 at 30 °C for 48 h. Substrate of 100% was converted to 2-methylbutanoic acid. After removal of all the volatiles in vacuo, a portion of the residue was chromatographed on a TLC plate (20 cm×20 cm×1 mm; eluent, a 4:1 $CHCl_3$/acetone) to give **4** (4.2 mg). The recovered **4** dissolved in $CDCl_3$ was subjected to ^{1}H NMR analysis. The intensities of the C(2) and C(3) protons and ee of the recovered **4** were virtually unchanged, indicating that (2*R*,3*R*)-**4**-*d*,*d* is isotopically stable.

Acknowledgements

This work was supported by a Grant-in-Aid for Scientific Research (Nos. 07CE2004, 05234101, 06226234, 08240101, 00000548, 60000491, and 9900481) from the Ministry of Education, Science, Sports and Culture, Japan. The authors would like to thank Professor R. Noyori for valuable discussions and Messrs. T. Noda, K. Oyama, and Y. Maeda for their technical support for reaction vessel production and NMR measurements.

Supplementary data

ORTEP drawings, tables of the atomic parameters, selected bond distances and bond angles, selected torsion angles, and anisotropic temperature factors for Ru[(*Z*)-$CH_3(C_6H_5)$C=CHCOO]$_2$[(*R*)-binap] are available (12 Pages). Supplementary data associated with this article can be found in the online version, at doi:10.1016/j.tet.2007.08.071.

References and notes

1. Arrhenius, S. *Z. Phys. Chem.* **1889**, *4*, 226–248.
2. The only exception: Kitamura, M.; Tsukamoto, M.; Bessho, Y.; Yoshimura, M.; Kobs, U.; Widhalm, M.; Noyori, R. *J. Am. Chem. Soc.* **2002**, *124*, 6649–6667.
3. (a) Sun, Y.; LeBlond, C.; Wang, J.; Blackmond, D. G.; Laquidara, J.; Sowa, J. R., Jr. *J. Am. Chem. Soc.* **1995**, *117*, 12647–12648; (b) Sun, Y.; Wang, J.; LeBlond, C.; Reamer, R. A.; Laquidara, J.; Sowa, J. R., Jr.; Blackmond, D. G. *J. Organomet. Chem.* **1997**, *548*, 65–72.
4. BINAP=2,2′-bis(diphenylphosphino)-1,1′-binaphthyl.
5. A similar type of double bond isomerization is also seen in the hydrogenation of arylalkenes mediated by a chiral phosphine/Ir

catalyst: Hou, D.-R.; Reibenspies, J.; Colacot, T. J.; Burgess, K. *Chem.—Eur. J.* **2001**, *7*, 5391–5400.
6. (a) Detellier, C.; Gelbard, G.; Kagan, H. B. *J. Am. Chem. Soc.* **1978**, *100*, 7556–7561; (b) Koenig, K. E.; Knowles, W. S. *J. Am. Chem. Soc.* **1978**, *100*, 7561–7564.
7. (a) Willoughby, C. A.; Buchwald, S. L. *J. Am. Chem. Soc.* **1994**, *116*, 8952–8965; (b) Willoughby, C. A.; Buchwald, S. L. *J. Am. Chem. Soc.* **1994**, *116*, 11703–11714.
8. Certain chiral substrates undergo racemization during reaction, allowing dynamic kinetic resolution. See: (a) Kitamura, M.; Tokunaga, M.; Noyori, R. *J. Am. Chem. Soc.* **1993**, *115*, 144–152; (b) Noyori, R.; Tokunaga, M.; Kitamura, M. *Bull. Chem. Soc. Jpn.* **1995**, *68*, 36–56.
9. Ishibashi, Y.; Bessho, Y.; Yoshimura, M.; Tsukamoto, M.; Kitamura, M. *Angew. Chem., Int. Ed.* **2005**, *44*, 7287–7290.
10. A report on a concept of the different pathways via same chain carrier: Sawamura, M.; Kuwano, R.; Ito, Y. *J. Am. Chem. Soc.* **1995**, *117*, 9602–9603.
11. Landis, C. R.; Halpern, J. *J. Am. Chem. Soc.* **1987**, *109*, 1746–1754.
12. This is not always the case, see Ref. 13.
13. Kitamura, M.; Yoshimura, M.; Tsukamoto, M.; Noyori, R. *Enantiomer* **1996**, *1*, 281–303.
14. Ohta, T.; Takaya, H.; Kitamura, M.; Nagai, K.; Noyori, R. *J. Org. Chem.* **1987**, *52*, 3174–3176.
15. Uemura, T.; Zhang, X.; Matsumura, K.; Sayo, N.; Kumobayashi, H.; Ohta, T.; Nozaki, K.; Takaya, H. *J. Org. Chem.* **1996**, *61*, 5510–5516.
16. For a similar double bond isomerization, see Refs. 2 and 6. The simplest type 2 substrate (*Z*)-3-methyl-d_3-2-butenoic acid also suffers from isomerization from α,β- to β,γ-unsaturated carboxylic acid.
17. (a) Ohta, T.; Takaya, H.; Noyori, R. *Inorg. Chem.* **1988**, *27*, 566–569; (b) Kitamura, M.; Tokunaga, M.; Noyori, R. *J. Org. Chem.* **1992**, *57*, 4053–4054.
18. Ashby, M. T.; Halpern, J. *J. Am. Chem. Soc.* **1991**, *113*, 589–594.
19. (a) Ashby, M. T.; Khan, M. A.; Halpern, J. *Organometallics* **1991**, *10*, 2011–2015; (b) Chen, C.-C.; Huang, T.-T.; Lin, C.-W.; Cao, R.; Chan, A. S. C.; Wong, W. T. *Inorg. Chim. Acta* **1998**, *270*, 247–251.
20. For the mechanism of the H/D exchange between RuH and CH_3OD and between RuH and D_2, see: (a) Jessop, P. G.; Morris, R. H. *Coord. Chem. Rev.* **1992**, *121*, 155–284; (b) Heinekey, D. M.; Mellows, H.; Pratum, T. *J. Am. Chem. Soc.* **2000**, *122*, 6498–6499.
21. The absolute configurations, 2*R*,3*S* and 2*S*,3*R*, are altered to 2*S*,3*S* and 2*R*,3*R* with the ^{13}C-nonlabeled 4-*d*,*h* and 4-*d*,*d*.
22. Corey, E. J.; Pasto, D. J.; Mock, W. L. *J. Am. Chem. Soc.* **1961**, *83*, 2957–2958.
23. (a) Noyori, R.; Kitamura, M. *Modern Synthetic Methods*; Scheffold, R., Ed.; Springer: Berlin, 1989; pp 115–198; (b) Noyori, R. *Asymmetric Catalysis in Organic Synthesis*; John Wiley: New York, NY, 1994; Chapter 2.
24. Clapham, S. E.; Hadzovic, A.; Morris, R. H. *Coord. Chem. Rev.* **2004**, *248*, 2201–2237.
25. For a molecular structure of $Ru(CH_3COO)_2$[(*R*)-binap]-(CH_3OH) in catalysis: see Ref. 2.
26. Ohta, T.; Takaya, H.; Noyori, R. *Tetrahedron Lett.* **1990**, *31*, 7189–7192.
27. Enamides: (a) Wiles, J. A.; Bergens, S. H. *Organometallics* **1998**, *17*, 2228–2240; (b) Wiles, J. A.; Bergens, S. H. *Organometallics* **1999**, *18*, 3709–3714; Other alkenes: (c) Ohta, T.; Ikegami, H.; Miyake, T.; Takaya, H. *J. Organomet. Chem.* **1995**, *502*, 169–176; (d) Schmid, R.; Broger, E. A.; Cereghetti, M.; Crameri, Y.; Foricher, J.; Lalonde, M.; Müller, R. K.; Scalone, M.; Schoettel, G.; Zutter, U. *Pure Appl. Chem.* **1996**, *68*, 131–138; (e) Bell, S.; Wüstenberg, B.; Kaiser, S.; Menges, F.; Netscher, T.; Pfaltz, A. *Science* **2006**, *311*, 642–644.
28. Lubell, D. W.; Kitamura, M.; Noyori, R. *Tetrahedron: Asymmetry* **1991**, *2*, 543–554.
29. Dihydride η^2-H_2: (a) Yu, J.; Spencer, J. B. *J. Am. Chem. Soc.* **1997**, *119*, 5257–5258; (b) Yu, J.; Spencer, J. B. *J. Org. Chem.* **1997**, *62*, 8618–8619; (c) Fong, T. P.; Lough, A. J.; Morris, R. H.; Mezzetti, A.; Rocchini, E.; Rigo, P. *J. Chem. Soc., Dalton Trans.* **1998**, 2111–2113.
30. Mechanistic study of asymmetric hydrogenation of α,β-unsaturated acids with diphosphine–Ru complexes: (a) Chan, A. S. C.; Chen, C. C.; Yang, T. K.; Huang, J. H.; Lin, Y. C. *Inorg. Chim. Acta* **1995**, *234*, 95–100; (b) Shaharuzzaman, M.; Chickos, J.; Tam, C. N.; Keiderling, T. A. *Tetrahedron: Asymmetry* **1995**, *6*, 2929–2932; (c) Hardick, D. J.; Blagbrough, I. S.; Potter, B. V. L. *J. Am. Chem. Soc.* **1996**, *118*, 5897–5903; (d) Shaharuzzaman, M.; Braddock-Wiking, J.; Chickos, J. S.; Tam, C. N.; Silva, R. A. G. D.; Keiderling, T. A. *Tetrahedron: Asymmetry* **1998**, *9*, 1111–1114.
31. The **4**-*d*,*d* isotopomer may be derived via the RuD species formed by the H/D exchange between RuH and CH_3OD, see: Bakos, J.; Karaivanov, R.; Laghmari, M.; Sinou, D. *Organometallics* **1994**, *13*, 2951–2956.
32. (a) Klein, J.; Turkel, R. M. *J. Am. Chem. Soc.* **1969**, *91*, 6186–6187; (b) Klein, J.; Aminadav, N. *J. Chem. Soc. C* **1970**, 1380–1385.
33. Almy, J.; Cram, D. J. *J. Am. Chem. Soc.* **1969**, *91*, 4459–4468.
34. Takahashi, H.; Fujiwara, K.; Ohta, M. *Bull. Chem. Soc. Jpn.* **1962**, *35*, 1498–1500.
35. Kudo, H.; Fujie, M.; Tanase, M.; Kato, M.; Kurosawa, K.; Sugai, H.; Umezawa, H.; Matsuzaki, T.; Nagamine, K. *Appl. Radiat. Isot.* **1992**, *43*, 577–583.
36. Hansen, P. E. *Annu. Rep. NMR Spectrosc.* **1984**, *15*, 105–234.